Physics Letters B 777 (2018) 406–411

Contents lists available at ScienceDirect

Physics Letters B

www.elsevier.com/locate/physletb

Pair production by three fields dynamically assisted Schwinger process

Ibrahim Sitiwaldi [a], Bai-Song Xie [a,b,*]

[a] Key Laboratory of Beam Technology of the Ministry of Education, and College of Nuclear Science and Technology, Beijing Normal University, Beijing 100875, China
[b] Beijing Radiation Center, Beijing 100875, China

ARTICLE INFO

Article history:
Received 4 April 2017
Received in revised form 28 December 2017
Accepted 28 December 2017
Available online 2 January 2018
Editor: A. Ringwald

ABSTRACT

The dynamically assisted Schwinger mechanism for vacuum pair production from two fields to three fields is proposed and examined. Numerical results for enhanced electron–positron pair production in the combination of three fields with different time scales are obtained using the quantum Vlasov equation. The significance of the combination of three fields in the regime of super low field strength is verified. Although the strengths of each of the three fields are far below the critical field strength, we obtain a significant enhancement of the production rate and a considerable yields in this combination, where the nonperturbative field is dynamically assisted by two oscillating fields. The number density depending on field parameters are also investigated. It is shown that the field threshold to detect the Schwinger effect can be lowered significantly if the configuration of three fields with different time scales are chosen carefully.

1. Introduction

After Dirac predicted the antiparticle of the electron, the positron, according to his famous equation, Sauter solved the Dirac equation for an electron in the Dirac sea in the presence of a static electric field to find a non-zero probability of electron–positron pair production from the vacuum under a strong static electric field [1]. Heisenberg and Euler derived the one-loop effective Lagrangian accounting for the coupling of a static electromagnetic field to the electron vacuum loop [2], according to which Schwinger calculated the electron–positron pair production rate in the presence of a static electric field [3]. Since then, vacuum pair production by electric fields has been usually referred to as the Schwinger effect.

The pair production rate in the Schwinger effect has a nonperturbative character due to its non-analytic field dependence. Therefore, it is of fundamental importance for our understanding of nonperturbative quantum field theories to study vacuum pair production. A large number of investigations are dedicated to study vacuum pair production, employing different methods such as proper time [4–6], WKB approximation [7], worldline instanton techniques [8,9], quantum field theoretical simulation [10–13] as well as the quantum kinetic method [14–19]. There is still no experimental verification of Schwinger pair production since the threshold field strength is too high to achieve in the laboratory at present, $E_{cr} = m^2c^3/e\hbar = 1.32 \times 10^{18}$ V/m (m and $-e$ denote mass and charge of electron, respectively).

In order to lower the electric field threshold to experimentally detect the Schwinger effect, various schemes have been proposed and among them the dynamically assisted Schwinger mechanism [20] is considered as the most promising one. In this scheme a greatly enhanced pair production rate is predicted, which also means a lower field threshold, in a slowly varying electric field superimposed by a rapidly oscillating one. The dynamically assisted Schwinger mechanism in a plane-wave x-ray probe beam superimposed by a strongly focused optical laser pulse [21], in the superposition of two periodic electric fields with a finite time interval [22] and in bifrequent fields [23–25] were also studied. The dynamically assisted Schwinger process in a spatially inhomogeneous field is also studied in [13]. More detailed investigations can be found in [26–28].

Unlike these schemes where various types of fields are considered but always with the combination of two fields, one fast-weak field and the other strong-slow/static field, there is an investigation where Schwinger process is doubly assisted by a perturbative weak field and a high energetic photon [29]. It is reasonable to expect further lower field threshold due to the combination of three fields with different time scales with the help of the dynamically

* Corresponding author at: Key Laboratory of Beam Technology of the Ministry of Education, and College of Nuclear Science and Technology, Beijing Normal University, Beijing 100875, China.
E-mail address: bsxie@bnu.edu.cn (B.-S. Xie).

https://doi.org/10.1016/j.physletb.2017.12.060

assisted Schwinger mechanism. Motivated by this, we present a comprehensive investigation on three fields dynamically assisted Schwinger mechanism in this paper. We employ quantum Vlasov equation for numerical calculation.

This paper is organized as follows: In Sec. 2 we introduce the theoretical formalism based on the quantum Vlasov equation. In Sec. 3 we analyze the numerical results. In the last section we provide a brief conclusion.

2. Quantum Vlasov equation for pair production process

Since the achievable spatial focusing scale is orders of magnitude larger than the Compton wavelength the spatial dependence of external field can be ignored. We also neglect the magnetic component in the external field as usual. The Schwinger pair production in a spatially homogeneous and time-dependent electric field $\mathbf{E}(t) = (0, 0, E(t))$, represented by a vector potential $\mathbf{A}(t) = (0, 0, A(t))$ where $E(t) = -\dot{A}(t)$, described by the quantum kinetic formalism based on the quantum Vlasov equation. In this formalism, the spectral information of produced particles is encoded in the distribution function $f(\mathbf{p}, t)$. It is necessary to remember that there is no clear interpretation of $f(\mathbf{p}, t)$ in the presence of an external field. At finite times it cannot be considered as distribution function of real particles but only as a mixture of real and virtual excitations. Consequently, $f(\mathbf{p}, t)$ might be interpreted as the momentum distribution for real particles only at asymptotic times $t = \pm\infty$, when the external field is switched off [30,31].

The equation of motion for $f(\mathbf{p}, t)$ is derived from canonical quantization with fully quantized spinor and the external electric field as a classical background [14]. We work in subcritical field regime $E \ll E_{cr}$ where the produced particle number density is so low that the collision effect and self consistent field current due to the produced particles can be neglected. With this simplifications, the quantum Vlasov equation for $f(\mathbf{p}, t)$ reads (we use natural units in this paper):

$$\dot{f}(\mathbf{p}, t) = \frac{1}{2} q(\mathbf{p}, t) \int_{-\infty}^{t} dt' q(\mathbf{p}, t')[1 - 2f(\mathbf{p}, t')] \cos[2\Theta(\mathbf{p}, t', t)], \tag{1}$$

where $f(\mathbf{p}, t)$ accounts for both spin directions due to absence of magnetic fields. Here, $q(\mathbf{p}, t) = eE(t)\varepsilon_\perp/\omega^2(\mathbf{p}, t)$ and $\Theta(\mathbf{p}, t', t) = \int_{t'}^{t} \omega(\mathbf{p}, \tau) d\tau$ with quantities as the electron/positron momentum $\mathbf{p} = (\mathbf{p}_\perp, p_\parallel)$, transverse energy squared $\varepsilon_\perp^2 = m_e^2 + p_\perp^2$, the total energy squared $\omega^2(\mathbf{p}, t) = \varepsilon_\perp^2 + p_\parallel^2$, and the longitudinal momentum $p_\parallel = P_3 - eA(t)$. This equation may be expressed as a linear, first order, ordinary differential equation system (ODEs) [15] for the convenience of numerical treatment:

$$\dot{f}(\mathbf{p}, t) = \frac{1}{2} q(\mathbf{p}, t) g(\mathbf{p}, t), \tag{2}$$

$$\dot{g}(\mathbf{p}, t) = q(\mathbf{p}, t)[1 - 2f(\mathbf{p}, t)] - 2\omega(\mathbf{p}, t) w(\mathbf{p}, t), \tag{3}$$

$$\dot{w}(\mathbf{p}, t) = 2\omega(\mathbf{p}, t) g(\mathbf{p}, t). \tag{4}$$

By numerically solving this ODEs with the initial conditions $f(\mathbf{p}, -\infty) = g(\mathbf{p}, -\infty) = w(\mathbf{p}, -\infty) = 0$, we can obtain the momentum distributions $f(\mathbf{p}, t)$ of the particles produced in the spatially homogeneous, time-dependent electric field. The number density $n(t)$ of created particles can be obtain by integrating $f(\mathbf{p}, t)$:

$$n(\infty) = 2 \int \frac{d^3\mathbf{p}}{(2\pi)^3} f(\mathbf{p}, \infty), \tag{5}$$

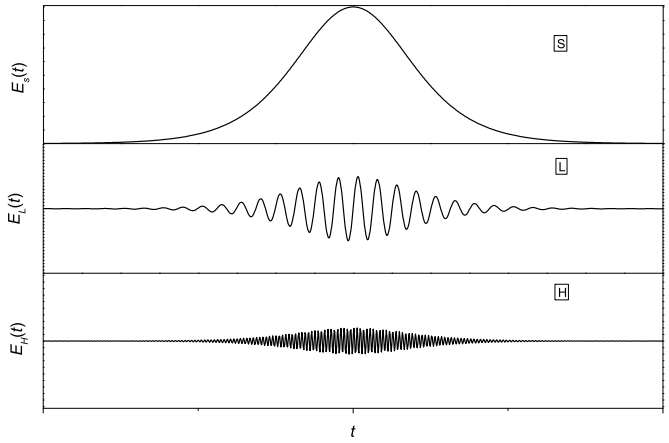

Fig. 1. Three fields with different time scales.

where the factor 2 comes from the degeneracy of electrons.

We fix the transverse momentum at $p_\perp = 0$ for simplicity in this paper.

3. Numerical results

3.1. Three fields with different time scales

We introduce a field configuration that is composed of a Sauter pulse (S), a lower frequency oscillating pulse (L) and a higher frequency oscillating pulse (H), as shown in Fig. 1. Their time dependence is given by:

$$E_S(t) = \frac{E_S}{\cosh^2(t/\tau_S)}, \tag{6}$$

$$E_L(t) = \frac{E_L}{\cosh^2(t/\tau_L)} \sin(\omega_L t), \tag{7}$$

$$E_H(t) = \frac{E_H}{\cosh^2(t/\tau_H)} \sin(\omega_H t), \tag{8}$$

where E_S, E_L and E_H denote the pulse strengths, τ_S, τ_L and τ_H denote the pulse durations of each field, ω_L and ω_H denote the oscillating frequencies of field L and H, respectively. The combination of the three fields (SLH) is represented as $E(t) = E_S(t) + E_L(t) + E_H(t)$.

In order to avoid trivial results we restrict $E_H \ll E_L \ll E_S$ and $\omega_L \ll \omega_H$.

3.2. Enhanced production rate in combination of SLH

We conduct large scaled numerical simulations for wide parameter space in the SLH fields and for each group of parameters we compare the produced particle number densities of each different composition, namely S, L, H, SL, SH, LH and SLH. In order to find a significance of the combination of three fields and lower the field strength as much as possible, we look for optimized parameters which maximize the increasing factors n_{SLH}/n_{SL}, n_{SLH}/n_{SH} and n_{SLH}/n_{LH} (n_{SLH} denotes the number density in SLH and so on) due to the combination of SLH.

According to our numerous calculations, the combination of three fields seems too trivial in the level of subcritical field strength ($E_S = 0.1E_{cr}$) where the combination of two fields works very well, however, it becomes essential in the level of super low field strength ($E_S = 0.01E_{cr}$), resulting a significantly enhanced production rate due to the combination of three fields. We discuss two group of optimized combination of three fields at first.

Table 1
Examples of optimized SLH.

Example	E_S/E_{cr}	E_L/E_{cr}	E_H/E_{cr}	ω_L/m	ω_H/m	γ_S	γ_L	γ_H
1	0.014	0.0020	0.00030	0.27	0.85	0.18	135	2800
2	0.014	0.0010	0.00005	0.33	1.60	0.18	330	32000

Table 2
Final number densities in different compositions of optimized SLH.

Example	S	L	H	SL	SH	LH	SLH
1	$\sim 10^{-103}$	$\sim 10^{-36}$	9.7×10^{-21}	$\sim 10^{-32}$	1.4×10^{-19}	9.8×10^{-21}	3.8×10^{-17}
2	$\sim 10^{-103}$	$\sim 10^{-34}$	2.1×10^{-17}	$\sim 10^{-31}$	2.7×10^{-17}	4.4×10^{-17}	3.7×10^{-13}

In Table 1 we represent the parameters of two examples of optimized SLH where the production rate is significantly enhanced due to the combination of three fields. The pulse durations are fixed at $\tau_S = \tau_L = \tau_H = \tau = 400\tau_0$, where $\tau_0 = 1/m$ denotes the electron Compton time. The strength of field S, L and H are lower than the critical value by two orders, three orders and four orders, respectively. The pair production mechanism is characterized by the Keldysh parameter of the external field:

$$\gamma = \frac{m\omega}{|eE|} = \frac{\omega E_{cr}}{m|E|}. \tag{9}$$

Here $\gamma \ll 1$ denotes the nonperturbative regime and $\gamma \gg 1$ denotes the multiphoton regime. In our examples γ_S is well in the nonperturbative regime whereas γ_L and γ_H are deep in the multiphoton regime as shown in the table (for the calculation of γ_S one can use $\omega_S = 1/\tau_S$).

Numerical errors in the simulation may occur when the simulation is performed in double or quad precision as usual adopted algorithm for some situations where the number density is too low. For these cases, however, we solve this problem by using the software package TIDES [33] in WOLFRAM MATHEMATICA which supports GNU MPFR [34] library for multiple precision calculation. This technique was successfully applied in related works [35,36] to precisely integrate ODEs with a great many number of significant digits.

In Table 2 we represent the produced number densities of each composition of SLH, for the two examples given above. In the example 1 the number density in SLH increases by two orders at least, compared to other compositions. In the example 2 the number density in SLH is increased by four orders, comparing to these compositions in the absence of each one component of SLH. The number densities in each single field component are rather small in both examples. Especially, the increasing factor due to the combination of SH is also rather low, $n_{SH}/n_H = 1.3$, which is a typical configuration for two field dynamically assisted Schwinger process.

The pair production rate is enhanced by several orders due to the combination of three fields with different time scales, which indicates the significance of the combination of three fields for certain parameters. Even more, we get considerable yields in the combination of SLH where the field strengths are far below the critical value. These results suggest that the generalization of dynamically assisted Schwinger mechanism from the combination of two fields to the combination of three fields can further lower the threshold for upcoming experiments.

3.3. Dependence of production rate on SLH parameters

To represent detailed characters of three field dynamically assisted Schwinger mechanism, we investigate the pair production rate in SLH depending on pulse durations, oscillating frequencies and field strengths, respectively. All parameters without a statement are the same as in example 2.

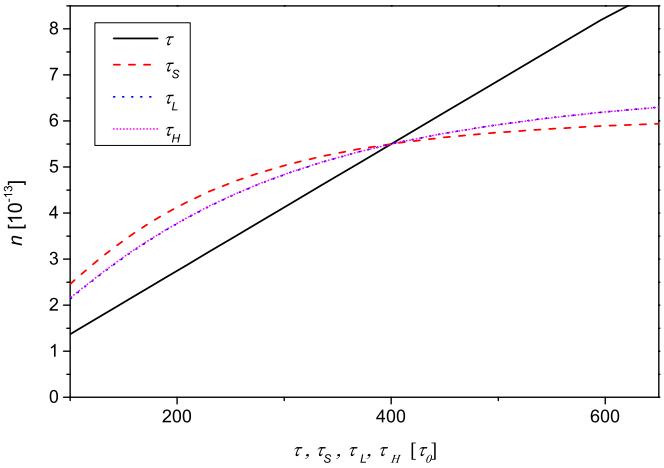

Fig. 2. (Color online.) Final yields in SLH as a function of pulse durations.

In Fig. 2 we study the final yields in SLH depending on pulse durations. In the case of pulse durations of each field component identical $\tau_S = \tau_L = \tau_H = \tau$ we get a straight line (solid line). The linear relation between the pulse duration and the final yields represents a continuous production rate within the pulse duration. We also study the influence of pulse duration of each single field while other two pulse durations are fixed at $400\tau_0$ (dashed color lines, lines of τ_L and τ_H coincide). The yields increase following with the pulse duration, but after it reaches $400\tau_0$ there is no clear increase. It is obvious that most pairs are produced when all of the three fields exist.

In Fig. 3 we display the final yields as a function of the oscillating frequencies ω_H and ω_L, respectively. In the upper panel, we fix ω_L at $0.23m$ and $0.33m$ and discuss the production yields depending on ω_H. It can be seen that there is a threshold for ω_H beyond which the production rate grows exponentially. The threshold is about $\omega_H = 1.50m$ and $\omega_H = 1.42m$ in the case of $\omega_L = 0.23m$ and $\omega_L = 0.33m$, respectively. The same results are also represented in the lower panel where the final yields as a function of ω_L is displayed. It indicates that there is certain threshold relation for the frequencies of two oscillating fields.

It is easy to see that after the frequency reaches its threshold the curve approaches a straight line in the logarithmic coordinate in the upper panel as well as in the lower panel in Fig. 3. It means that the production rate as a function of ω_H and ω_L can be approximated by an exponential function as soon as the frequencies reach corresponding thresholds to trigger three fields dynamically assisted Schwinger process. So we can estimate the production rate as

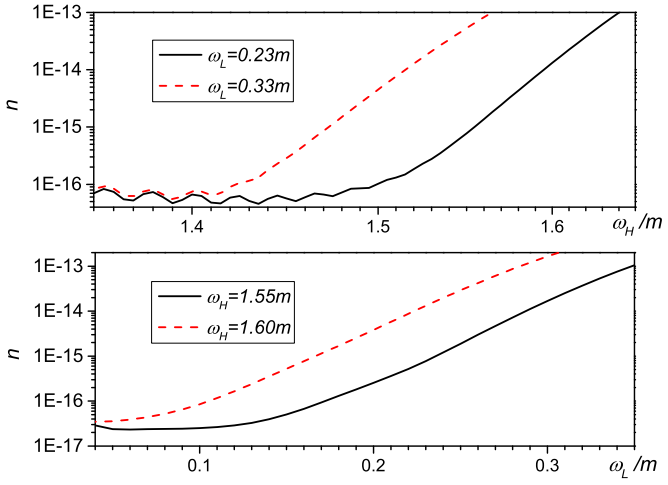

Fig. 3. (Color online.) Final yields in SLH as a function of oscillating frequencies ω_H and ω_L, respectively.

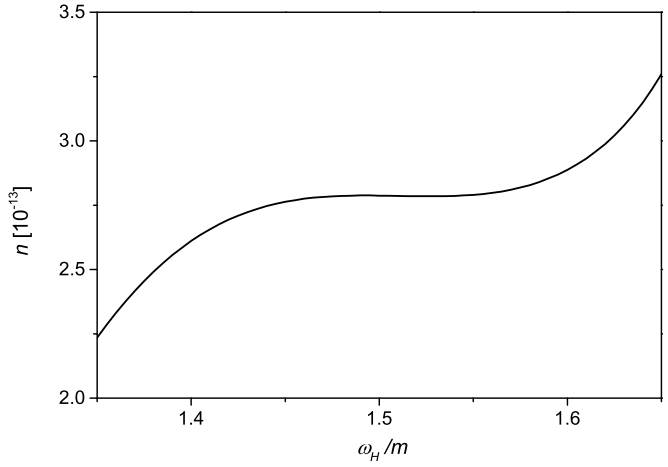

Fig. 4. Final yields as a function of ω_H with $22\omega_H + 17\omega_H = 41m$.

$$\Gamma \propto e^{a\omega_H + b\omega_L}, \tag{10}$$

where $a = 22/m$ and $b = 17/m$ for present case according to the data. To check this relation further we investigate the final yields as a function of ω_H while both of ω_H and ω_L are changing but $22\omega_H + 17\omega_L$ keeps unchanged (we chose $\omega_H = 1.60m$ and $\omega_L = 0.33m$ as a reference point so that $22\omega_H + 17\omega_L = 41m$) in Fig. 4. The final yields almost keeps unchanged in a area of $1.40m < \omega_H < 1.63m$, as we expected. Eq. (10) is helpful to optimize our scheme but it can not be taken too serious since it is only a rough approximation of numerical results.

In Fig. 5 we display the final yields as a function of E_S for different ω_H. The final yields begin to grow by orders only when E_S exceeds a threshold, which is 0.0045 for $\omega_H = 1.55m$ and 0.0020 for $\omega_H = 1.60m$, respectively. It means that there is also a threshold for E_S which is determined by the gap left behind by the photon energy of perturbative field to overcome. However, in the case of $\omega_H = 1.67$, the production rate is always very high compared to the other two cases and the influence of E_S is minor. It is because the photon energy is just enough ($\omega_H + \omega_L = 2m$) so that the contribution of the Schwinger tunneling process with too low field strength is negligible.

From findings in Fig. 3 and Fig. 5 we can demonstrate that a threshold relation satisfied by the total photon energy of oscillating fields and the potential energy of non-perturbative field is essential to the production rate in the combination of three fields.

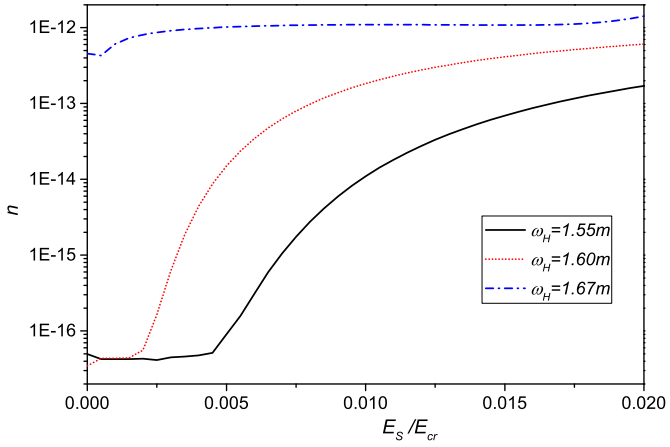

Fig. 5. (Color online.) Final yields as a function of E_S for different ω_H.

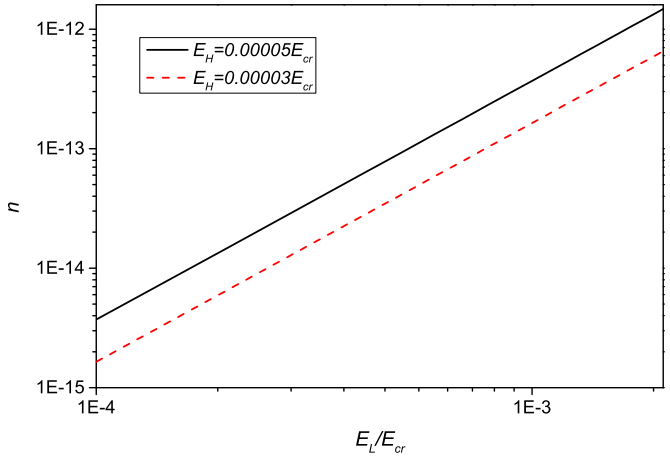

Fig. 6. (Color online.) Final yields as a function of E_L for different E_H.

The production rate as a function of the amplitude of the oscillating fields with an amplitude E and a frequency ω in the perturbative regime is given by $\Gamma \simeq (\frac{|eE|}{2m\omega})^{4m/\omega}$ [32]. It gives the production rate in threshold frequency for n photon process as $\Gamma \simeq (\frac{|eE|}{2m\omega})^{2n}$, by this we can write down the dependence of the production rate on E_H and E_L for example 2 as

$$\Gamma \propto E_L^2 E_H^2. \tag{11}$$

To check this relation we display the final yields as a function of E_L for different E_H in Fig. 6. We get perfect straight lines in the logarithmic axes, fitting well with a power function with index just 2 for both case. The similar investigation with E_H also gives the same results and we ignore to display it.

3.4. Momentum distributions in SLH

In Fig. 7 we display the longitudinal momentum distributions of the particles produced in H, LH, SH and SLH for the example 2, the momentum distributions in the other compositions are too low to display.

In the case of H and LH, the momentum of produced particles is well defined by the energy momentum relation as we expect, where the pair energy is determined by the photon energy of the oscillating fields. In the case of SH, the momentum distributions is

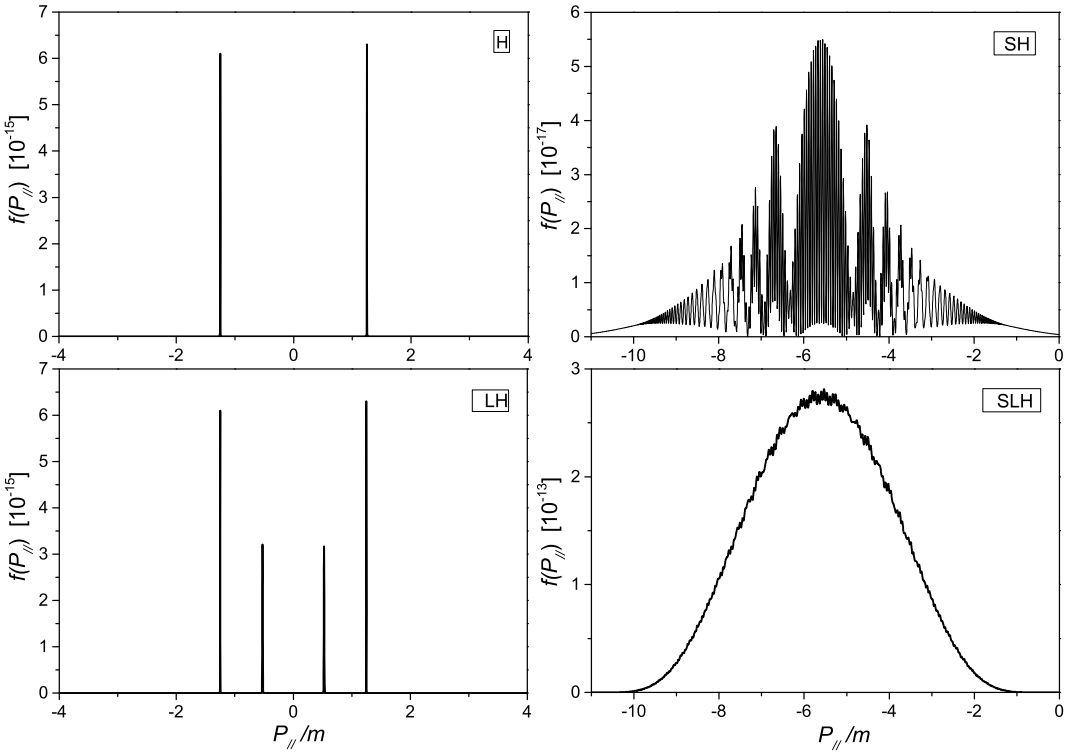

Fig. 7. The longitudinal momentum distributions of the electrons produced in each composition of SLH for the example 2.

lower and wider than in the case of H since the produced electrons is continuously accelerated by the nonperturbative field S. In the case of SLH, the momentum distributions are enhanced by several orders compared to the other cases.

Except the distributions height, another significant difference there is that the momentum distributions is discrete in the case of SH while it is continuous (with small oscillation) in the case of SLH. Unlike in the multiphoton regime, in the presence of a nonperturbative field the momentum of a particle is determined by its creation time, the earlier time it is created the longer time it has to be accelerated by the nonperturbative field and the higher longitudinal momentum it gets at final. This assumption also can be supported by the result in [26]. So the discrete momentum distributions in the case of SH indicates the discrete pair production rate in time. In the same way, the continuous momentum distributions in the case of SLH indicates a continuous production rate in time and it also implies a higher final production rate in the combination of SLH.

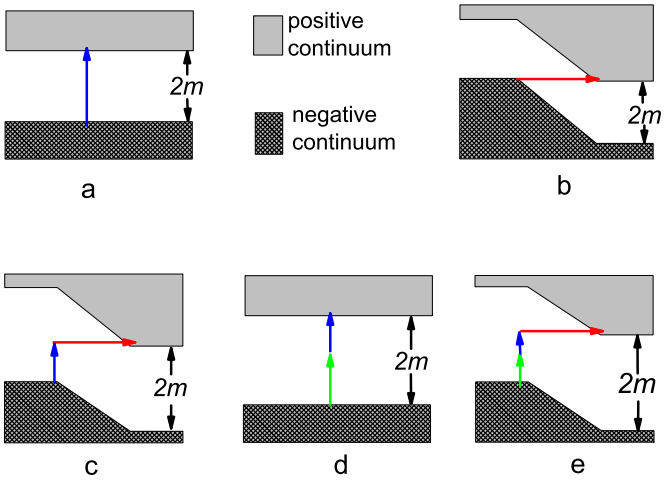

Fig. 8. (Color online.) Pictures of different pair production mechanisms.

3.5. Dynamically assisted Schwinger mechanism in SLH

In Fig. 8 we illustrate different pair production mechanisms. Panel a and b illustrate the well-known mechanism of multiphoton process and Schwinger tunneling process, respectively. Panel c illustrates the dynamically assisted Schwinger process in the combination of a nonperturbative field and a perturbative field [26]. Panel d illustrates pair production triggered by a combination of different photons in a bifrequent field [24]. Panel e illustrates the dynamically assisted Schwinger process in the combination of one nonperturbative field and the other two perturbative fields, which is the main achievement of this paper.

4. Conclusion

The electron–positron pair production process in the combination of three fields with different time scales in super low field strength is investigated and the main results are represented in this paper. Two groups of optimized field parameters chosen via large scale numerical simulations are illustrated where considerable yields are obtained in the combination of the three fields, even though the field strengths are far below the critical field strength. By comparing the production yields in each composition of the three fields it is demonstrated that the production rate can be enhanced significantly due to the combination of three fields for certain parameters. The influence of field parameters on production rate and the significant differences in the momentum distributions in each field composition are also discussed. Some relations between the pair production rate and field parameters are estimated and it is demonstrated that a threshold relation satisfied by the total photon energy of oscillating fields and the potential energy of non-perturbative field is essential to the production rate

in the combination of three fields. The enhancement of the production rate due to the combination of three fields is attributed to three fields dynamically assisted Schwinger mechanism where the nonperturbative field is dynamically assisted by two oscillating fields.

Our investigation indicates that it is possible to experimentally detect the Schwinger effect even for very low field strength with the help of dynamically assisted Schwinger mechanism by reasonably superimposing more than two fields with different time scales. The three fields dynamically assisted Schwinger mechanism needs to be studied further for different types of fields.

Acknowledgements

We enjoyed several helpful discussions with Suo Tang, and Feng Wan. Authors are also grateful to the anonymous referee for the helpful suggestions to improve the quality of manuscript. This work was supported by the National Natural Science Foundation of China (NSFC) under Grant No. 11475026.

References

[1] F. Sauter, Z. Phys. 69 (1931) 742.
[2] W. Heisenberg, H. Euler, Z. Phys. 98 (1936) 714.
[3] J.S. Schwinger, Phys. Rev. 82 (1951) 664.
[4] R.G. Newton, Phys. Rev. 96 (1954) 523.
[5] W.Y. Tsai, A. Yildiz, Phys. Rev. D 8 (1973) 3446.
[6] V.N. Baier, V.M. Katkov, V.M. Strakhovenko, Sov. Phys. JETP 40 (1974) 225.
[7] S.P. Kim, D.N. Page, Phys. Rev. D 65 (2002) 105002.
[8] G.V. Dunne, C. Schubert, Phys. Rev. D 72 (2005) 105004.
[9] G.V. Dunne, Q.H. Wang, H. Gies, C. Schubert, Phys. Rev. D 73 (2006) 065028.
[10] T. Cheng, Q. Su, R. Grobe, Contemp. Phys. 51 (2010) 315.
[11] P. Krekora, K. Cooley, Q. Su, R. Grobe, Phys. Rev. Lett. 95 (2005) 070403.
[12] Q.Z. Lv, Y. Liu, Y.J. Li, R. Grobe, Q. Su, Phys. Rev. Lett. 111 (2013) 183204.
[13] M. Jiang, W. Su, Z.Q. Lv, X. Lu, Y.J. Li, R. Grobe, Q. Su, Phys. Rev. A 85 (2012) 033408.
[14] Y. Kluger, E. Mottola, J.M. Eisenberg, Phys. Rev. D 58 (1998) 125015.
[15] J.C.R. Bloch, et al., Phys. Rev. D 60 (1999) 116011.
[16] R. Alkofer, et al., Phys. Rev. Lett. 87 (2001) 193902.
[17] C.D. Roberts, S.M. Schmidt, D.V. Vinnik, Phys. Rev. Lett. 89 (2002) 153901.
[18] N. Abdukerim, Z.L. Li, B.S. Xie, Phys. Lett. B 726 (2013) 820.
[19] I. Sitiwaldi, B.S. Xie, Phys. Lett. B 768 (2017) 174.
[20] R. Schützhold, H. Gies, G. Dunne, Phys. Rev. Lett. 101 (2008) 130404.
[21] G.V. Dunne, H. Gies, R. Schützhold, Phys. Rev. D 80 (2009) 111301.
[22] A. Otto, D. Seipt, D. Blaschke, B. Kämpfer, S.A. Smolyansky, Phys. Lett. B 740 (2014) 335.
[23] Martin J.A. Jansen, Carsten Müller, Phys. Rev. A 88 (2013) 052125.
[24] I. Akal, S. Villalba-Chávez, C. Müller, Phys. Rev. D 90 (2014) 113004.
[25] A. Otto, D. Seipt, D. Blaschke, S.A. Smolyansky, B. Kämpfer, Phys. Rev. D 91 (2015) 105018.
[26] M. Orthaber, F. Hebenstreit, R. Alkofer, Phys. Lett. B 698 (2011) 80.
[27] Z.L. Li, D. Lu, B.S. Xie, et al., Phys. Rev. D 89 (2014) 093011.
[28] A. Nuriman, B.S. Xie, Z.L. Li, D. Sayipjamal, Phys. Lett. B 717 (2012) 465.
[29] Greger Torgrimsson, Johannes Oertel, Ralf Schützhold, Phys. Rev. D 94 (2016) 065035.
[30] Robert Dabrowski, Gerald V. Dunne, Phys. Rev. D 90 (2014) 025021.
[31] Robert Dabrowski, Gerald V. Dunne, Phys. Rev. D 94 (2016) 065005.
[32] V.S. Popov, J. Exp. Theor. Phys. 34 (1972) 709.
[33] A. Abad, R. Barrio, F. Blesa, M. Rodriguez, ACM Trans. Math. Softw. 39 (2012) 1.
[34] L. Fouse, G. Hanrot, V. Lefevre, P. Pelissier, P. Zimmermann, ACM Trans. Math. Softw. 33 (2007) 13.
[35] C. Schneider, R. Schützhold, Phys. Rev. D 94 (2016) 085015.
[36] G. Torgrimsson, C. Schneider, J. Oertel, R. Schützhold, J. High Energy Phys. 06 (2017) 043, arXiv:1703.09203.